# Simvastatin-hydroxyapatite coatings prevent biofilm formation and improve bone formation in implant-associated infections

Tiantong Sun [a,b,c], Jie Huang [a,b,c], Wang Zhang [a,b,c], Xuanqi Zheng [a,b,c], Hong Wang [a,b,c], Jing Liu [d], Huijie Leng [a,b,c], Wanqiong Yuan [a,b,c], Chunli Song [a,b,c,*]

[a] Department of Orthopedics, Peking University Third Hospital, Beijing, China
[b] Beijing Key Laboratory of Spinal Diseases, Beijing, China
[c] Engineering Research Center of Bone and Joint Precision Medicine, Ministry of Education, Beijing, China
[d] Institute of Medical Sciences, The Second Hospital of Shandong University, Jinan, China

ABSTRACT

Implant-associated infections (IAIs) caused by biofilm formation are the most devastating complications of orthopedic surgery. Statins have been commonly and safely used drugs for hypercholesterolemia for many years. Here, we report that simvastatin-hydroxyapatite-coated titanium alloy prevents biofilm-associated infections. The antibacterial properties of simvastatin against *Staphylococcus aureus* and *Staphylococcus epidermidis* biofilms *in vitro* was confirmed by crystal violet staining and live-dead bacterial staining. We developed a simvastatin-and-hydroxyapatite (Sim-HA)-coated titanium alloy via electrochemical deposition. Sim-HA coatings inhibited *Staphylococcus aureus* biofilm formation and improved the biocompatibility of the titanium alloy. Sim-HA coatings effectively prevented *Staphylococcus aureus* IAI in rat femurs, as confirmed by radiological assessment and histological examination. The antibacterial effects of the Sim-HA coatings were attributed to their inhibitory effects on biofilm formation, as verified by scanning electron microscopic observations and bacterial spread plate analysis. In addition, the Sim-HA coatings enhanced osteogenesis and osteointegration, as verified by micro-CT, histological evaluation, and biomechanical pull-out tests. In summary, Sim-HA coatings are promising implant materials for protection against biofilm-associated infections.

## 1. Introduction

Implant-associated infections (IAIs) are the primary cause of complications following implantation and have devastating consequences. In America, IAIs account for 50% of the 2 million cases of nosocomial infections that occur each year, causing high rates of morbidity and mortality and substantial hospitalization costs [1–3]. The most prevalent pathogen in orthopedic IAI is *Staphylococcus aureus* (*S. aureus*), which is a highly opportunistic pathogen that can form biofilms on implant surfaces [1,2].

Biofilm formation on the surface of orthopedic implants is considered the main cause of IAI that are difficult to eradicate [1,4]. Biofilms are a highly dense group of microorganisms wrapped in a hydrated matrix for synthesis [5,6]. Biofilms develop preferentially on inert surfaces and commonly occur in medical devices, especially on metal-based materials that are widely used as orthopedic implants. Biofilms are

extremely resistant to antibiotics and host immune defense, leading to difficulties in eradication [5]. Current clinical strategies to prevent and treat IAI include systemic administration of antibiotics and implant removal surgery. However, systemic administration of antibiotics cannot effectively prevent the occurrence of IAI [5]. For example, the local concentration of antibiotics may be low because of the existence of a "blood-bone barrier" [7]. In addition, biofilm formation increases the resistance of bacteria to antibiotics [8].

Statins are cholesterol-lowering drugs that have been used safely in clinical practice for decades. Recently, the pleiotropic effects of statins have been investigated, including the effects on osteogenesis, angiogenesis, immune regulation, and anti-inflammatory activity [9–12]. Studies indicate that statins exhibit antibacterial ability owing to the direct influence of bacterial growth and biofilm formation by destroying functional membrane microdomains [13]. In addition, a series of previous studies have demonstrated the osteogenic ability of simvastatin

both *in vitro* and *in vivo* [14,15]. The primary target organ of statins is the liver; less than 5% of orally administered statins reach systemic circulation after the first-pass hepatic metabolism, and even lower concentrations are found in the skeleton [16]. Local application of simvastatin can recruit autogenous stem cells and promote osteogenesis in osteoporosis and related fracture models [15,17–19].

In this study, we developed simvastatin-hydroxyapatite-coated Ti6Al4V implants. The antibacterial effects and biocompatibility of Sim-HA-Ti6Al4V were examined *in vitro*. Using the rat IAI model, the antibacterial and osteogenic effects of sim-HA implants were evaluated *in vivo*.

## 2. Materials and methods

### 2.1. Examination of the minimum inhibitory concentration of simvastatin

Standard strains of *Staphylococcus epidermidis* (*S. epidermidis*) and *Staphylococcus aureus* (*S. aureus*) were used to test the minimum inhibitory concentration (MIC) of simvastatin. *ATCC 35984* and *ATCC 25923* were purchased from the Guangdong Microbial Culture Collection Center. *ATCC 25923* is a methicillin-sensitive strain, and is the standard strain used for antimicrobial susceptibility testing according to the Clinical and Laboratory Standards Institute. *ATCC 35984* is methicillin-resistant. Both strains are biofilm-forming strains [20]. The MIC was tested by the broth microdilution method established by the Clinical and Laboratory Standards Institute [21,22]. After overnight incubation of *S. epidermidis* and *S. aureus*, bacterial fluid with 0.5 McFarland standard and broth microdilution method was used to test the MIC of simvastatin. The lowest concentration of simvastatin that could completely inhibited the visible growth of bacteria after 16 h of incubation at 37 °C in a 96-well plate was considered the MIC.

### 2.2. Anti-biofilm effects of simvastatin in vitro

The inhibition of biofilm formation by simvastatin and the disruption of mature biofilms of *S. epidermidis* and *S. aureus* were then examined by 0.1% (wt/vol) crystal violet staining (Solarbio G1063, China) and bacterial live-dead staining (Invitrogen L13152, USA) using confocal laser-scanning microscopy (Zeiss 800. Germany). The intensity of crystal violet staining was evaluated by optical density (OD) value at 595 nm ($OD_{595}$) using microplate reader (Tecan Infinite 200 PRO, Switzerland) [21,23]. The $OD_{595}$ of the biofilm in the group not treated with simvastatin was treated as a control (inhibition and disruption rates were 0%), and the inhibition and disruption rates of groups treated with different concentrations of simvastatin were then calculated.

### 2.3. Preparation of Sim-HA-Ti6Al4V implants

Ti6Al4V implants (Wego, China) were roughened as previously described [24]. Ti6Al4V samples (discs of 10 mm diameter and 1.5 mm thickness used for *in vitro* experiments, rods of 1.5 mm diameter and 20 mm height used for *in vivo* experiments) were polished using sandpapers, sonicated in acetone, 75% ethanol, and distilled water, and then air-dried. The samples were then treated with a solution of HF/HNO$_3$ for 10 min at room temperature and then treated with a solution of HCl/H$_2$SO$_4$ for 30 min at 80 °C.

**S**imvastatin (Yuanye Bio-Technology, China) solution was prepared as previously described [25,26]. Briefly, 42 mg simvastatin was dissolved in 1 ml 95% ethanol. Then 1.5 ml of 0.1 M NaOH was added. The solution was heated at 50 °C for 2 h and then was neutralized to pH 7.2 with 0.1 M HCl. Deionized water was then added to reach a volume of 10 ml. Simvastatin acid (10 mM) was then prepared.

The HA coatings were prepared according to previous studies with modifications [24,25,27]. Ti6Al4V was used to make the working electrode (cathode) and the counter electrode was a platinum plate. The electrolytes contained analytical grade 0.6 mM Ca (NO$_3$)$_2$ (Aladdin, China) and 0.36 mM Ca (NO$_3$)$_2$ (Aladdin, China) dissolved in distilled water. The Ca/P ratio of the solution was 1.67 and the pH was adjusted to 6.0. To improve the conductivity of the electrolyte, NaNO$_3$ was added at a final concentration of 0.1 M. The electrochemical deposition process was conducted using a DC power source at 1.5 V at 85 °C for 30 min. The same process was performed to conduct simvastatin-hydroxyapatite (Sim-HA) coatings on the Ti6Al4V samples, with the only difference being that $10^{-4}$ and $10^{-3}$ mol/L simvastatin was added to the electrolyte solution. These two Sim-HA-coated samples were named Sim-Low and Sim-High.

### 2.4. Material characterization

#### 2.4.1. Surface characterization

The surface morphologies of the different implants were examined using field-emission scanning electron microscopy (SEM, Hitachi SU8100, Japan). The crystal structures of the coatings on the different implants were characterized by X-ray diffraction (XRD, Bruker D8, Germany) with Cu K radiation. The chemical composition of CaP deposition was characterized by Fourier-transform infrared spectroscopy (FTIR, Nicolet iS10, USA) using the KBr pellet technique. Contact angle tests were performed to evaluate the biocompatibility of the implant materials using a contact angle measuring instrument (Biolin Theta Flex, Sweden). The roughness of the implant surface was evaluated using three-dimensional (3D) laser microscopy (Keyence VK-150K, Japan). Surface area roughness (Sa) and 3D topographical images were also calculated. The bonding strength between coatings and substrate was tested by nano scratch test (CSM Micro-Scratch Tester, Swiss) with progressive loading mood of normal force from 1 to 100 N over a scratch length of 5 mm. The bonding strength was recorded by the critical normal force which caused detachment of coatings.

#### 2.4.2. Concentration analysis

Concentration analysis of simvastatin integrated into the Sim-HA coatings was conducted as reported in previous studies [24,25]. Briefly, Sim-HA-Ti6Al4V plates were immersed in 2 ml phosphate buffer solution (PBS, pH 7.4), and 200 μL of the samples were transferred into 1.5 ml polypropylene tube containing 600 μL methanol (Sinopharm Chemical Reagent, China). The tubes were vortexed for 60 s and then centrifuged at 13000 rpm for 5 min. The supernatant was collected for liquid chromatography-electrospray tandem mass spectrometry (LC-MS/MS) analysis. Quantification of simvastatin was performed using multiple reaction-monitoring modes at m/z 435.87 → 319.58. A $10^{-2}$ mol/L simvastatin solution was used as the standard. Sample concentrations were calculated by comparing the absorption peak of the multiple reaction monitoring mode with that of the standard sample.

#### 2.4.3. Simvastatin release test

The drug release process of Sim-HA-Ti6Al4V was evaluated according to previous studies, with modifications [26,28–30]. Sim-Low and Sim-High plates were placed into 5 ml falcon cubes containing 2 ml PBS. The samples were incubated at 37 °C with constant stirring at 70 rpm. Once the defined time elapsed, samples of the medium were collected. The concentration of simvastatin was measured using an ultraviolet–visible microplate reader (Biotek Cytation 5, USA) and an ultraviolet–visible 96-well plate (Solarbio YA0602, China) at 238 nm. Standard solutions of simvastatin were used to obtain the standard curve, which showed a linear relationship between UV absorbance and drug concentration. The measurements were performed in triplicates. The percentage release of simvastatin was calculated as the released concentration divided by the total concentration integrated in the Sim-HA coatings.

### 2.5. Antibacterial effect of Sim-HA-Ti6Al4V in vitro

The inhibitory effect of simvastatin on *S. aureus* biofilm formation

was then examined by live-dead bacterial staining with confocal laser-scanning microscopy [31]. SEM scanning was also conducted to evaluate the morphology of the bacteria and their biofilms on the coated materials and the pristine Ti4Al6V alloy.

According to previous studies [28,31], the spread plate assay was performed to quantitatively evaluate the antibacterial effect of Sim-HA-Ti6Al4V *in vitro*. After culturing *S. aureus* on plates for 24 h, the adherent bacteria attached to the disc samples were collected ultrasonically (50HZ, 5 min) in PBS after vortexing rapidly for 1 min. The bacterial suspensions were serially diluted and plated onto tryptone soy agar plates for overnight culturing. The number of colonies on the plates was counted, and the number of bacteria that adhere on disc samples was calculated and recorded.

### 2.6. Biocompatibility evaluation of Sim-HA-Ti6Al4V

Bone mesenchymal stem cells (BMSCs) of Sprague-Dawley (SD) rat were purchased from Cyagen Biosciences (China). BMSCs were seeded at a density of $5 \times 10^4$ cells/mL (0.5mL/well) onto Ti6Al4V disc samples placed in a 24-well culture plate [32]. Samples were washed with PBS and stained with phalloidin-iFluor 594 (Abcam 176757, USA) to visualize the cytoskeleton of the cells 24 h after seeding. Nuclei were stained with DAPI solution (Solarbio C0065, China), followed by observation using confocal laser-scanning microscopy. Cell proliferation was evaluated using a CCK-8 assay (Dojindo CK04, Japan). The results of the CCK-8 test were expressed as relative cell proliferation rates by normalizing the OD450 values to those of the control group on day 1. BMSCs were seeded on four groups of 24-well plates and incubated with osteogenic differentiation medium (Cyagen Biosciences RAXMX-90021, China) for 14 days. The osteogenic differentiation of rBMSCs was then evaluated via alkaline phosphatase (ALP) activity test using an ALP kit (Beyotime, China) according to the manufacturer's protocol.

### 2.7. Antibacterial effect of Sim-HA-Ti6Al4V in vivo

A rat IAI model was employed to estimate the anti-infection effect of Sim-HA-Ti6Al4V according to previous operation procedures [33–35]. The Ethics Committee of the Second Hospital of Shandong University approved all animal experimental protocols (Project No.: KYLL-2021 (KJ) A-0416).

Forty-eight adult male SD rats (10 weeks old) were randomly assigned to four groups, namely, control, HA, Sim-low, and Sim-high, consistent with the four different implants. Briefly, 50 μL of the ATCC 25923 bacterial suspension at a concentration of $1 \times 10^5$ colony forming units (CFUs)/mL was injected into the medullary cavity of the right femur. Rods were then implanted into the right distal femur of rats. The body weights of the rats in the four groups were measured weekly. The number of the white blood cells in the four groups of rats was tested at 1, 2, and 6 weeks after surgery. After 1,3 and 6 weeks, lateral radiographs were obtained to observe infected femurs and knee joints. Radiographic scores were evaluated according to previous studies [32,33,36] as follows:1, periosteal reaction; 2, osteolysis; 3, soft tissue swelling; 4, deformity; 5, general impression; 6, spontaneous fracture; 7, sequestrum formation. Parameters 1 to 5 were recorded as follows: 0, absent; 1, mild; 2, moderate; and 3, severe. Parameters 6 and 7 were scored as 0 (absent) or 1 (present). The radiographs were read and interpreted by two radiologists who were blinded to the grouping characteristics. The plasma concentrations of interleukin-6 (IL-6) and tumor necrosis factor-α (TNF-α) were determined using enzyme-linked immunosorbent assay (ELISA) at 1, 2, and 6 weeks after surgery to evaluate the changes in inflammatory cytokines in the four groups of IAI rats.

Six weeks after implantation, the rats were sacrificed and the femurs were harvested for sterilization. The CFU counts of bacteria on the implant surface were counted by the spread plate method as previously described [33]. The rod implants were removed from the femurs and scanned using SEM to evaluate bacterial and biofilm morphology on the

surface of the implants. Transverse and longitudinal decalcified sections of the distal femurs without implants were obtained from the same levels as the distal femurs. Histological evaluation of the antibacterial effects was then performed with hematoxylin and eosin (HE) staining and Giemsa staining. To evaluate the biosafety of HA and Sim-HA coatings on implants, HE staining was performed to observe the morphologies of five rat organs, namely, the heart, liver, spleen, lung, and kidney, in four groups.

#### 2.7.1. Evaluation of osteogenesis in vivo

*2.7.1.1. Double fluorescent labeling.* The rats were injected with 20 mg/kg calcein green (Sigma, USA) via the tail vein 14 and 4 days before euthanasia [37]. The undecalcified sections of right distal femur around the implants were obtained (EXAKT Cutting & Grinding System, Germany) [9,38]. The mineral apposition rate (MAR) was calculated using confocal microscopy by measuring the mean distance between two fluorescent labels.

#### 2.7.2. Micro-CT analysis

Six weeks after implantation, the rats in the four different groups were sacrificed, and the right femurs with implants were scanned by micro-CT (PerkinElmer Quantum GX2, USA) at 90 kV and 88 μA. Three-dimensional images of the distal femur in the four groups were reconstructed using a 20 μm voxel size. New bone formation around the implants was evaluated in the area 1 mm below the epiphyseal line of the distal femur [39]. Trabecular bone parameters, including bone volume/tissue volume (BV/TV), trabecular number (Tb.N), trabecular thickness (Tb.Th), and trabecular separation (Tb.sp), were analyzed and compared among the four groups.

#### 2.7.3. Biomechanical pull-out test

Six weeks after implantation, the strength of implant fixation was evaluated using a biomechanical push-out test and a mechanical testing system (MTS Landmark Servohydraulic Test System, MN, USA). As previously described [19,40], specimens were embedded in polymethyl methacrylate and implants were pulled out along the longitudinal axis of the implants. The biomechanical push-out test was performed at a rate of 5 mm/min, with a preload force of 5 N. The maximum value of the ultimate load was recorded.

#### 2.7.4. ELISA

The bone resorption marker, tartrate-resistant acid phosphatase 5b (TRAcP 5b), and the bone formation marker, N-terminal propeptide of type 1 procollagen (P1NP), were quantified by ELISA at 6 weeks after surgery to evaluate bone turnover using immunoassay kits in accordance with the manufacturer's instructions (Elabsceince, China). Two other osteogenic markers, osteopontin (OPN) and bone alkaline phosphatase (BALP), were also evaluated using ELISA 6 weeks after surgery.

### 2.8. Statistical analysis

All data are presented as mean ± standard deviation (SD). All statistical analyses were performed using the GraphPad Prism software (version 8.0). One-way or two-way ANOVA followed by a post-hoc Tukey's test was performed to determine the statistical significance between groups. Statistical significance was set at $P \leq 0.05$.

## 3. Results

### 3.1. Antibacterial effects of simvastatin in vitro

*S. aureus* and *S. epidermidis* are the pathogens that most frequently cause orthopedic infections. First, we examined the antibacterial effects of simvastatin against two biofilm-positive strains (*S. aureus ATCC*

*25923* and *S. epidermidis ATCC 35984*). The MICs of simvastatin against *ATCC 25923* and *ATCC 35984* was 64 μg/ml. At the MIC, simvastatin significantly inhibited biofilm formation, according to the results of crystal violet staining with evaluation of $OD_{595}$ (Fig 1A, C) and live-dead staining with confocal laser-scanning microscopy (Fig. 1E, G). Furthermore, simvastatin exhibited a strong ability to disrupt mature biofilms of *S. aureus* and *S. epidermidis in vitro* compared to the control groups (Fig. 1B, D). At a concentration of 256 μg/ml, the biofilm was partially disrupted, and the number of live bacteria decreased, as observed by laser scanning microscopy (Fig. 1F, H).

### 3.2. Characterization of Sim-HA-Ti6Al4V

The surface morphologies of Sim-HA-Ti6Al4V and the other materials were examined using SEM. After polishing, the control group exhibited a porous structure on the surface of the Ti6Al4V alloy. The Ti6Al4V-HA and the other two Sim-HA-Ti6Al4V exhibited similar surface coating morphologies. Rod-like crystals covered the surface of the material (Fig. 2A). The XRD pattern of the coating showed that the coating exhibited typical apatite peaks at 2θ of approximately 25.9 °C and 31–33 °C, which matched standard HA patterns (Fig. 2B). Furthermore, the FTIR spectra of the coatings showed that they consisted of HA crystals (Fig. 2C). The stretching band of the $OH^-$ group appeared at approximately 3566 $cm^{-1}$. The bands of $PO_4^{3-}$ appeared at
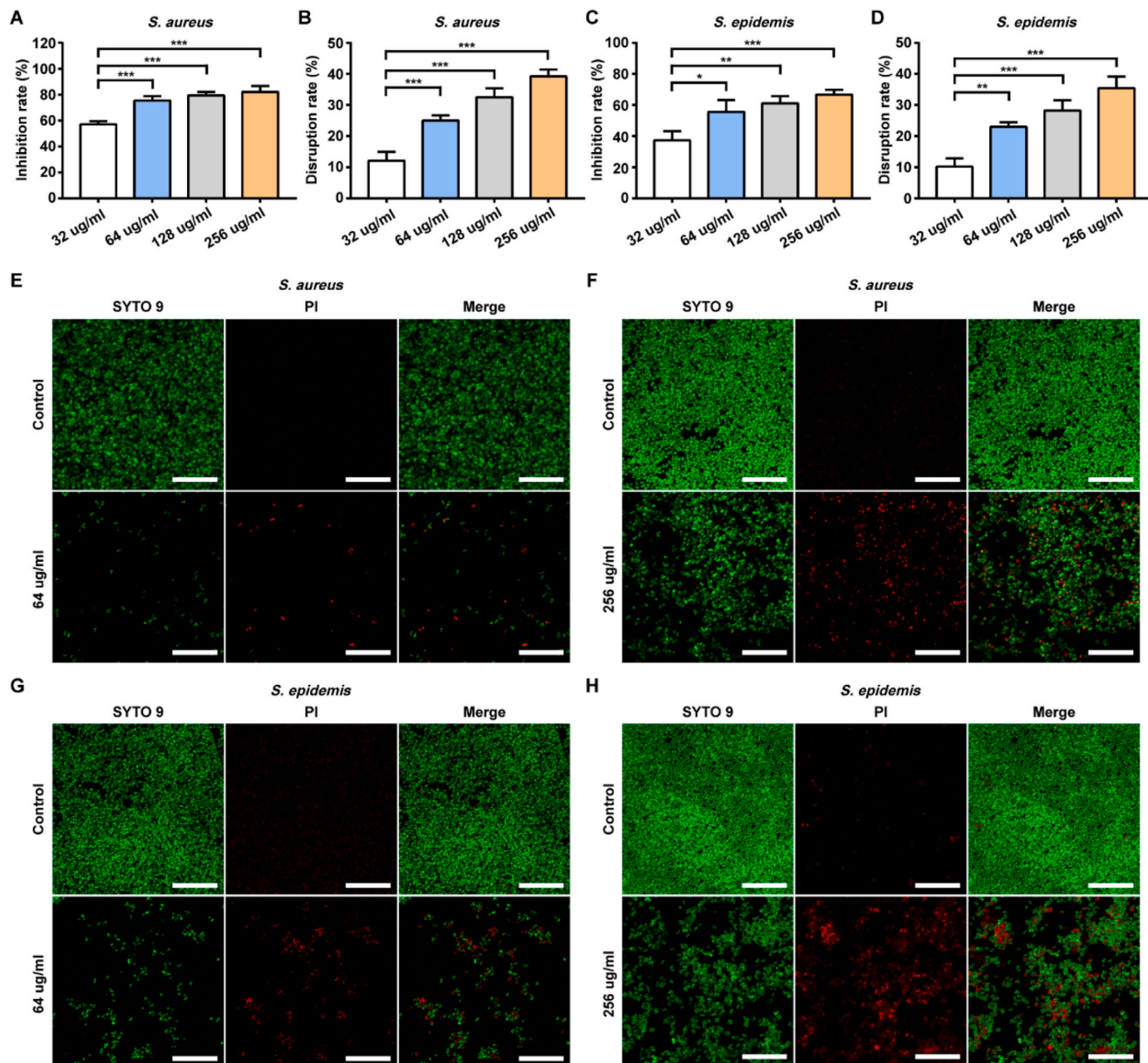


**Fig. 1.** Effects of simvastatin on biofilm inhibition and disruption.
**A-D** *S. aureus* and *S. epidermis* were treated with simvastatin at different concentrations for 24 h. The inhibition effect and disruption effect were measured by crystal violet staining. Data are shown as the mean ± SD, n = 3, * for P < 0.05, ** for P < 0.01, *** for P < 0.001. **E-H** Confocal fluorescence images showed *S. aureus* and *S. epidermis* biofilms after 24 h of treatment with simvastatin at different concentrations. Live cells were stained green and dead cells were stained red. Scale bar: 20 μm.
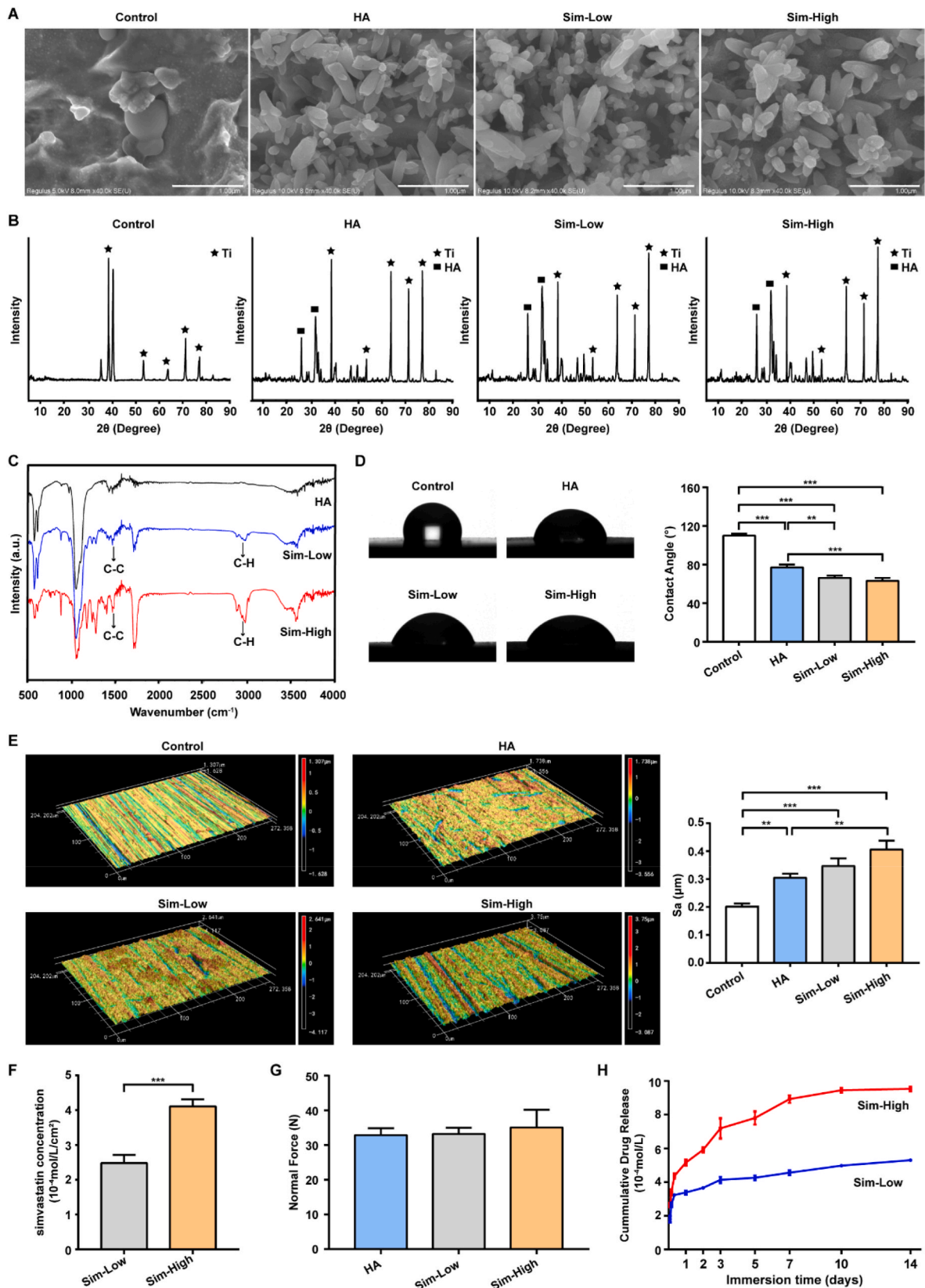
**Fig. 2.** Characterization and properties of Sim-HA-Ti6Al4V.
**A** SEM micrograph of uncoated or coated Ti6Al4V with HA and different concentrations of simvastatin. Scale bar: 1 μm. **B** XRD patterns of HA precipitation and Ti precipitation. **C** FTIR spectra of Ti6Al4V coated with HA and different concentrations of simvastatin. **D** Representative images and statistics of contact angles in four groups. **E** Representative topographical images of surfaces determined by 3D laser microscopy and statistics of surface area roughness (Sa) in four groups. **F** Concentration analysis of simvastatin in two Sim-HA coatings by LC-MS/MS. **G** Bonding strength (Normal Force) of HA and Sim-HA coatings. **H** The cumulative drug release profiles for two Sim-HA coatings. Data are shown as the mean ± SD, n = 3, ** for $P < 0.01$, *** for $P < 0.001$.

$1042 \, \text{cm}^{-1}$ and $1091 \, \text{cm}^{-1}$, $566 \, \text{cm}^{-1}$ and $603 \, \text{cm}^{-1}$. The C–H stretching vibration bands at $2930 \, \text{cm}^{-1}$ and $2955 \, \text{cm}^{-1}$ and the C–C vibration bands at approximately $1472 \, \text{cm}^{-1}$ indicated simvastatin. The contact angles of the four materials were also examined. Based on these results, it can be inferred that simvastatin was incorporated into the synthetic HA coating. To evaluate the biocompatibility of Sim-HA-Ti6Al4V, we used a contact angle assay. Pristine Ti6Al4V, HA-Ti6Al4V, and Sim-HA-Ti6Al4V were used as the control for HA, Sim-Low, and Sim-High groups, respectively. The contact angles of the Sim-Low and Sim-High groups were significantly smaller than those of the control and HA groups, indicating that the Sim-HA coatings improved the biocompatibility of the Ti6Al4V alloy (Fig. 2D).

The roughness values of the four implant types were tested. Representative 3D topographical images of the surface in the different groups are shown in Fig. 2E. The roughness parameter of the surfaces (Sa) of the HA, Sim-Low, and Sim-High groups were significantly higher than that of the control group. Additionally, the roughness of the Sim-High group was significantly higher than that of the HA group. There were no significant differences between the bonding strength of HA and Sim-HA groups (Fig. 2G). The concrete pictures of the four different rod and disc implants are shown in Fig. S1.

### 3.3. Simvastatin release of Sim-HA-Ti6Al4V

To determine the concentration of simvastatin in the Sim-HA coatings in the Sim-Low and Sim-High groups, LC-MS was conducted. According to the results, the concentration of simvastatin in Sim-Low and Sim-high group were $2.483 \pm 0.2354 \times 10^{-4} \, \text{mol/L/cm}^2$ and $4.112 \pm 0.2033 \times 10^{-4} \, \text{mol/L/cm}^2$, respectively (Fig. 2F). The drug release assay showed that simvastatin in the Sim-HA coatings exhibited a burst release over 50% of the total concentration in the first 24 h (Fig. 2H). For both the Sim-Low and Sim-High groups, at an immersion time of 2 h, the concentrations of simvastatin were above the MIC. After burst release in the first 24 h, simvastatin was released slowly over 14 days.

### 3.4. In vitro anti-infection evaluation of Sim-HA-Ti6Al4V

Anti-infection evaluation of Sim-HA-Ti6Al4V was conducted using a live-dead *in vitro* staining assay of *ATCC 25923*, assessed using confocal laser-scanning microscopy. The results showed that both the Sim-Low and Sim-High groups exhibited greater inhibition of bacterial growth and biofilm formation than the HA and control groups (Fig. 3A). The SEM results also showed fewer bacteria or less biofilm formation on the Sim-Low and Sim-High implant surfaces than on the surface of the HA and control implants (Fig. 3B). The quantitative antibacterial results of the spread plate assay are shown in Fig. 3C. Fewer bacteria adhered on the implants of the Sim-coated groups than in the control and HA groups. In addition, there were fewer adherent bacteria in the HA group than in the control group. These results indicate that Sim-HA coatings inhibit bacterial adhesion, growth, and biofilm formation on the surface of implants.

### 3.5. In vitro biocompatibility evaluation of Sim-HA-Ti6Al4V

To further validate the biocompatibility of the different materials, we seeded SD rat BMSCs on the surfaces of the materials *in vitro*. After 24 h of incubation, cytoskeleton staining showed that the cells on Sim-HA-Ti6Al4V and Ti6Al4V-HA were fully attached to the materials and exhibited superior expansion morphologies when compared with the surface of the pristine Ti6Al4V control group (Fig. 3D). These results suggest that the HA and Sim-HA coatings of the Ti6Al4V alloy can promote the attachment and expansion of BMSCs on the surface of the materials. The CCK8 results also indicated that Sim-HA-Ti6Al4V could significantly increase the proliferation of BMSCs compared to that of the control group (Fig. 3E). The ALP activity assay showed that the BMSCs seeded on HA- and Sim-HA-coated Ti6Al4V exhibited higher ALP

activity than those seeded on the control group (Fig. 3F).

### 3.6. In vivo anti-infection evaluation of Sim-HA-Ti6Al4V

The body weights of the Sim-Low and Sim-High groups were significantly higher than those of the control and HA groups at 5 and 6 weeks after surgery (Fig. 4A). We observed that body weight decreased slightly at 2 weeks after surgery and then started to increase slowly with time, indicating that none of the four groups of rats emaciated after surgery (Fig. 4A). After the first week of surgery, the number of WBCs reached the highest level among the three time points and then decreased to within normal level at 6 weeks (Fig. 4B). Obvious signs of bone infection, including periosteal reactions and osteolysis, were detectable on radiographs in the control and HA groups 3 weeks after surgery. Six weeks after surgery, these signs became obvious with the progression of bone destruction of the femur and knee joint. The radiology scores of the Sim-Low and Sim-High groups were significantly lower than those of the control and HA groups (Fig. 4C). However, mild or no signs of bone infection were observed in the Sim-Low and Sim-High groups (Fig. 4D).

The plasma levels of inflammatory cytokines in the four groups were evaluated using ELISA. As shown in Fig. 4E–F, both IL-6 and TNF-α levels in plasma were significantly higher in the control and HA groups than in the Sim-Low and Sim-High groups, 1 and 2 weeks after IAI surgery. Six weeks after implantation, the implants in the four groups were removed for SEM scanning and bacterial counting assay. The number of live bacteria on the different implants was counted using the spread plate method. Representative images of the plates in the four groups are shown in Fig. 4G. The CFU numbers in the control and HA groups were significantly higher than those in the Sim-Low and Sim-High groups (Fig. 4H). The SEM results showed the aggregation morphology of *S. aureus* on the surface of the implants in both the control and HA groups. In contrast, fewer bacteria were present on the surfaces of the two Sim-coated groups (Fig. 4I).

Morphological changes in longitudinal and transverse decalcified slices were assessed using HE staining (Fig. 5A). The results also validated the similar antibacterial properties of the Sim-Low and Sim-High groups compared to that of the control and HA groups. The cortical bone of the distal femur of the rats in the control and HA groups exhibited severe osteolysis and bone resorption. In contrast, the Sim-Low and Sim-High groups exhibited fewer signs of infection around implants. The longitudinal and transverse morphologies of the femurs in the Sim-High group were almost normal, without signs of infection. Giemsa staining showed large amounts of bacteria in the cortical bone of the femur in the control and HA groups. There were few bacteria in the Sim-HA group and no bacteria were observed in the Sim-High group. The results in Fig. 5B show that there were no morphological abnormalities in the five organs of rats in the four groups, indicating good biosafety of the HA and Sim-HA coatings. Among the results above, the Sim-HA-coated Ti6Al4V alloy exhibited antibacterial ability *in vivo*.

### 3.7. In vivo osteogenesis evaluation of Sim-HA-Ti6Al4V

Micro-CT analysis of the distal femur around the implants was conducted to evaluate the osteogenic properties of the different implants at 6 weeks. Images of the median sagittal and transverse sections of rat femurs are shown in Fig. 6A–B. The cortical bone and knee joint morphologies in the Sim-Low and Sim-High groups were better than those in the other two groups. BV/TV and Tb.N in the Sim-Low and Sim-High groups were significantly higher than those in the control and HA groups (Fig. 6C–D). In addition, the mean Tb.Th of the Sim-Low and Sim-High groups were higher than that of the other two groups, but a statistically significant difference was observed only between the Sim-High and HA groups (Fig. 6E). Additionally, there were no significant differences in Tb.Sp among the four groups (Fig. 6F). Osteogenesis was evaluated by double calcein green labeling with confocal fluorescence
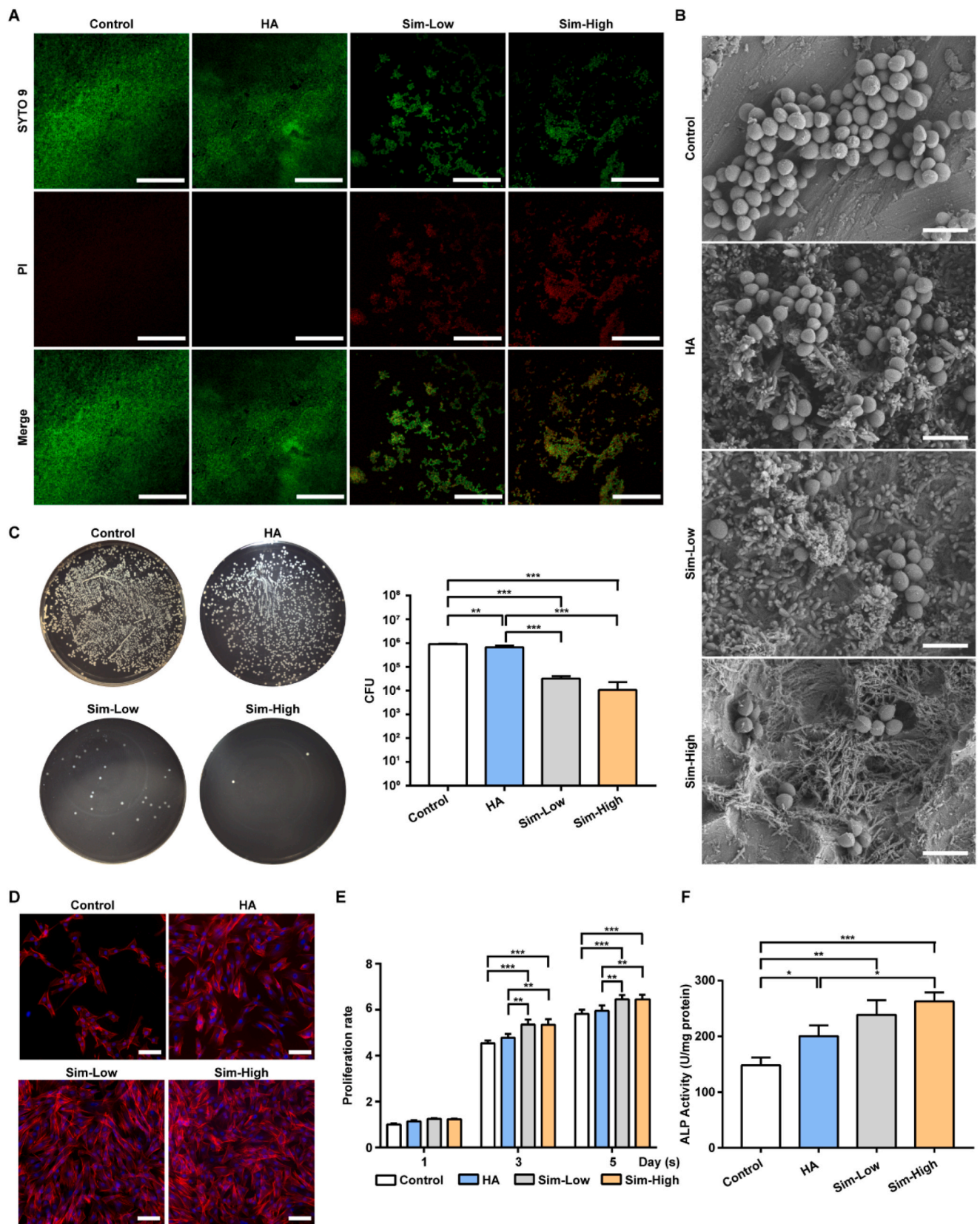
**Fig. 3.** Antibacterial effect and biocompatibility of Sim-HA-Ti6Al4V.

**A** Confocal fluorescence images of Ti6Al4V, Ti6Al4V-HA and Sim-HA-Ti6Al4V for *S. aureus* biofilm formation by laser confocal microscopy, scale bar: 50 μm. B SEM images of four implants for *S. aureus* biofilm formation, scale bar: 2 μm. **C** Images and statistics of spread plate assay. **D** Rat BMSCs adhesion on different four implants, scale bar: 50 μm. **E** Proliferation rate of rat BMSCs grown on the four different implants. **F** ALP activity of BMSCs on four implants. Data are shown as the mean ± SD, n = 3. * for P < 0.05. ** for P < 0.01, *** for P < 0.001.
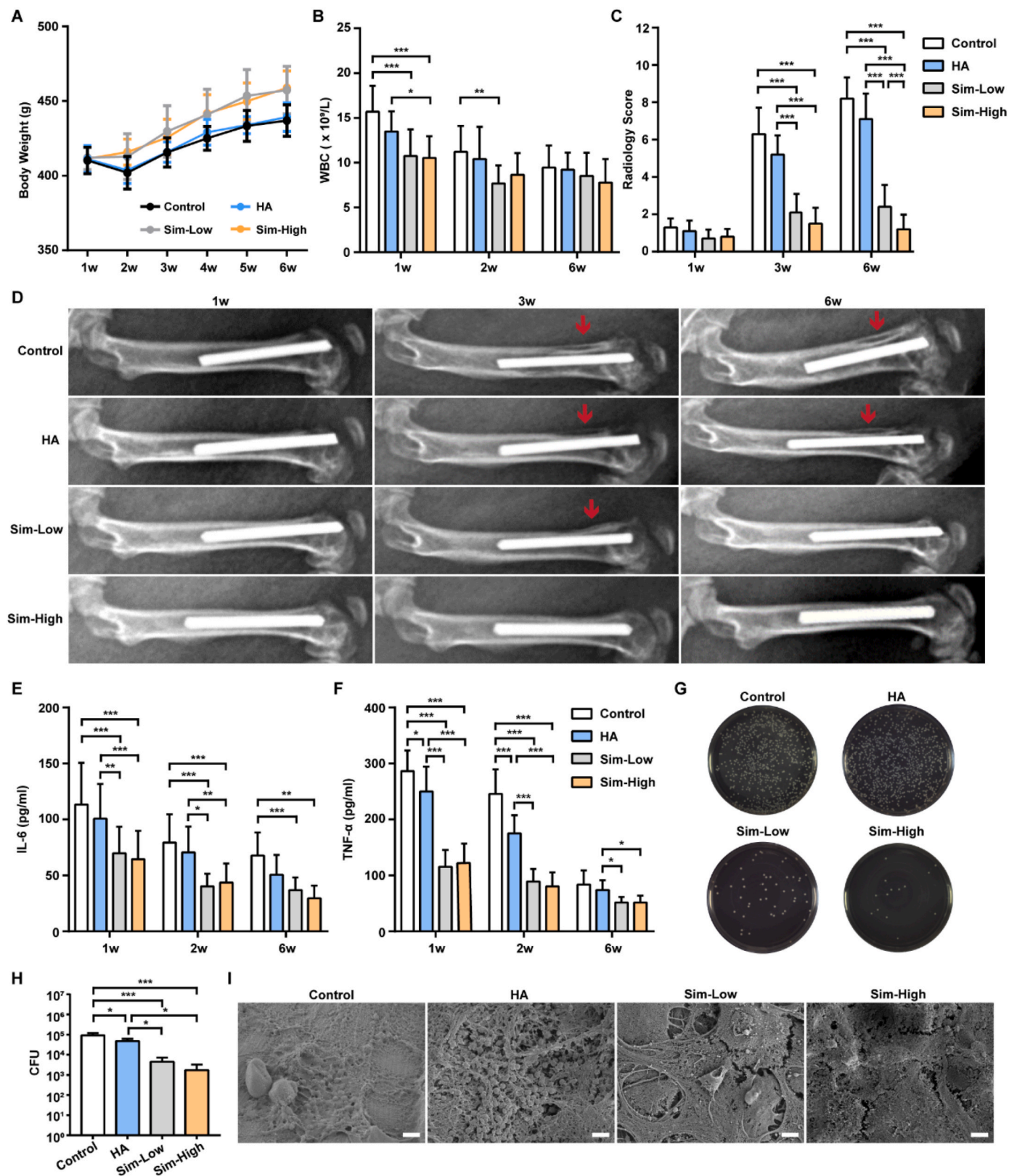
**Fig. 4.** Antibacterial evaluation of Sim-HA-Ti6Al4V *in vivo*.
**A** Changes in the body weights of the rats in the four groups during the 6 weeks after surgery. **B** Changes in rat blood WBCs in the four groups at 1 w, 2 w, and 6 w after surgery. **C** Radiology scores of X-rays of four groups at 1 w, 3 w, and 6 w after surgery (n = 10). **D** Representative images of rat femur at 1 w, 3 w, and 6 w after surgery. The red arrows indicate destruction of the cortical bone of the distal femur. **E-F** Plasma concentrations of IL-6 and TNF-α in rats in the four groups at 1 w, 2 w, and 6 w after surgery. **G** Culture of bacteria released from four different implants. **H** Quantitative analysis of released bacteria from four different implants (n = 3). **I** SEM images of four different implants 6 w after surgery, scale bar:2 μm. Data are shown as the mean ± SD, n = 12. *for $P < 0.05$, ** for $P < 0.01$, *** for $P < 0.001$.
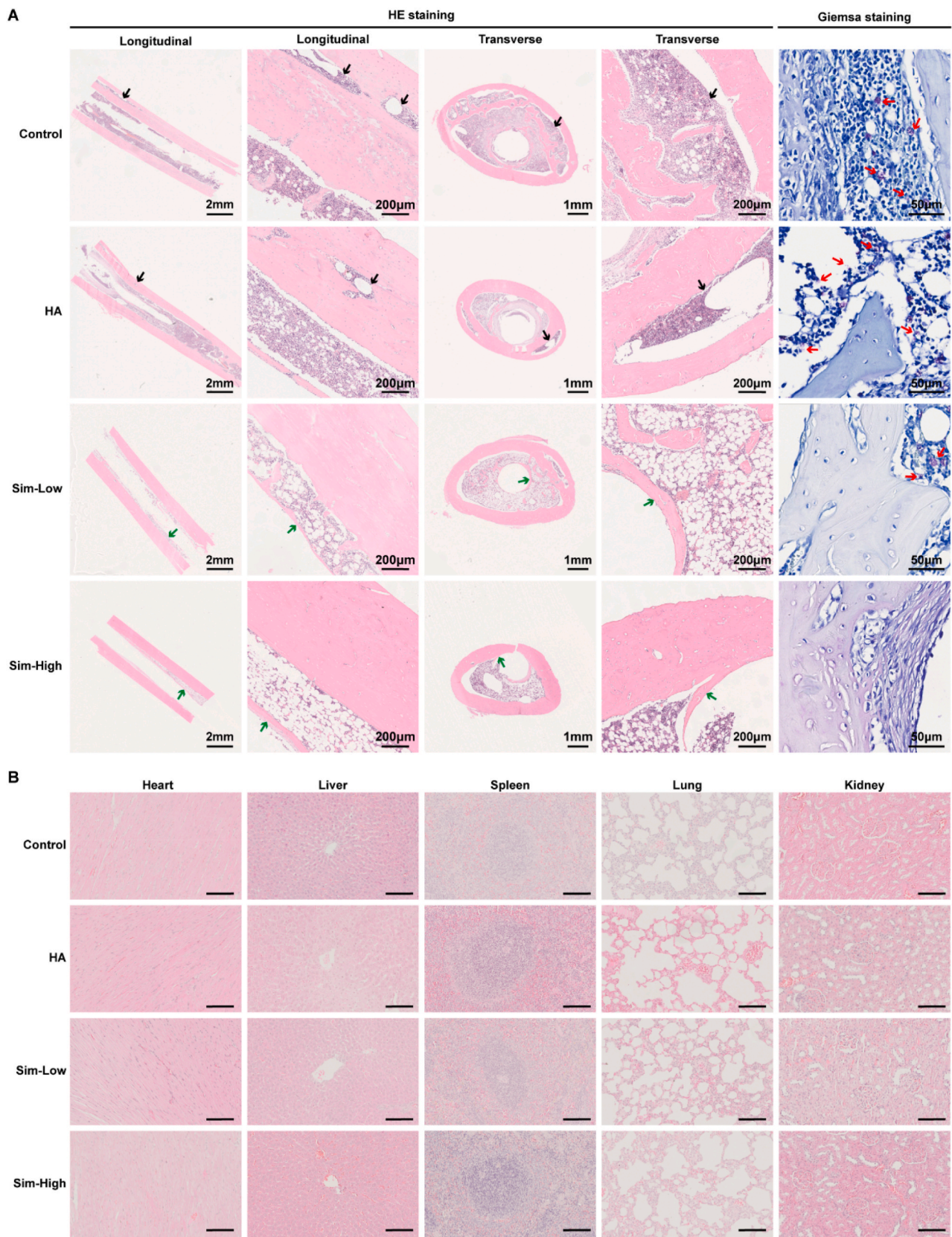
**Fig. 5.** Histological evaluation of the Sim-HA-Ti6Al4V *in vivo*.
**A** Representative histological images of hematoxylin and eosin staining and Giemsa staining of rat femurs. The black arrows represent massive destruction of cortical bone. The green arrows indicate new bone formation around implants. The red arrows indicate bacteria remaining in the bone tissue. **B** Hematoxylin and eosin staining analyses of different organs, including the heart, liver, spleen, lung, and kidney. n = 3.

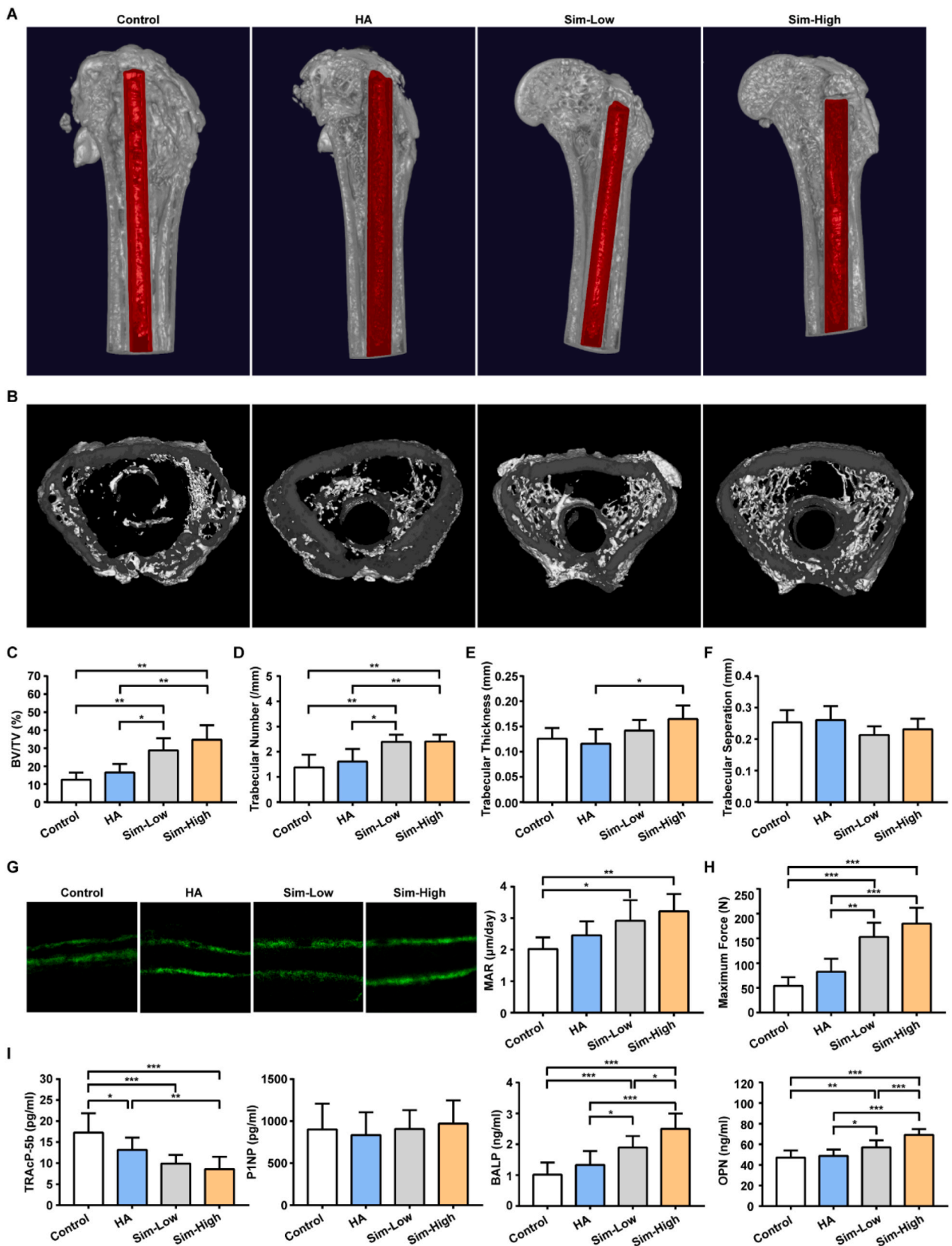microscopy, followed by MAR analysis. Representative images of the control, HA, Sim-Low, and Sim-High groups are shown in Fig. 6G. MAR was calculated by measuring the distance between the two labels. Osteointegration of implants in the four groups was evaluated using a biomechanical pull-out test. The results showed that the maximum forces of the Sim-Low and Sim-High groups were significantly higher than those of the Control and HA groups.

The plasma level of the bone absorption marker TRAcP-5b was significantly lower in the Sim-Low and Sim-High groups than in the control and HA groups 6 weeks after surgery (Fig. 6I). OPN and BALP levels of the Simvastatin groups were significantly higher than those of the control and HA groups. Additionally, OPN and BALP levels in the Sim-High group were significantly higher than those in the Sim-Low group. However, no significant differences were found when comparing the plasma levels of the bone formation marker P1NP among the four groups (Fig. 6I).

## 4. Discussion

In the present study, we found that simvastatin exhibited antibacterial and osteogenic properties in implant-associated infections (IAIs). Simvastatin inhibited bacterial growth and formation of *S. epidermidis* and *S. aureus* biofilms *in vitro*. Sim-HA coatings could inhibit bacterial adhesion and biofilm formation of *S. aureus* while improving the biocompatibility of the materials used. In addition, Sim-HA coatings on Ti–6Al–4V prevented IAI and improved osteogenesis in a rat IAI model.

IAIs are one of the most devastating complications and remain a major challenge in orthopedic surgery. IAI with titanium-based implants remains a significant challenge. Efforts have been directed toward the development of new biomaterials with both anti-infection and biocompatibility properties to prevent and treat IAI [30,41–50]. Prophylactic application of antibiotics as coatings on biomaterials seems to be an effective method to prevent infections directly. Álvaro. et al. constructed a fluorine- and phosphorus-doped nanostructured Ti6Al4V alloy coated with vancomycin and gentamicin to prevent *S. aureus* induced IAI in a rabbit model. Some studies have used 3D porous scaffolds to load traditional antibiotics. Zhang. et al. evaluated the effects of vancomycin-loaded in micro-arc oxidized 3D printed Ti6Al4V scaffolds for treating Methicillin-resistant *Staphylococcus aureus* (MRSA) induced bone infection and osteogenesis [51]. Although some new strategies had developed the controlled and sustainable release of antibiotics to avoid the toxicity effects of drug burst release, the widespread use of antibiotics induced antimicrobial-resistant strains more frequently.

Statins are a family of 3-hydroxy-3-methylglutaryl-CoA reductase inhibitors that have been widely used clinically as cholesterol-lowering drugs for decades. In the 1970s, Akira Endo speculated that fungi could produce antibiotics to interfere with each other's cholesterol synthesis and first isolated statins in the secretion compounds of *Penicillium citrinum* [52]. Recent studies have found that statins also exhibit antibacterial properties against various bacterial strains, including *S. epidermidis*, *S. aureus* and even *methicillin-resistant Staphylococcus aureus* (MRSA) [13,21,53–56]. Simvastatin, which is listed as an OTC drug in many countries, has been widely used for its efficacy and safety in reducing cholesterol levels in clinical practice for over 40 years. Abundant *in vivo* studies have demonstrated the positive effect of simvastatin on bone formation [17,18,57,58]. Therefore, in the present study, we examined the antibacterial effects of simvastatin *in vitro*. The minimum inhibitory concentrations of simvastatin against *ATCC 35984* and *ATCC 25923* were consistent with that reported for *S. epidermidis* and *S. aureus* in previous studies [21].

Biofilm formation on implants is the primary characteristic of IAI. Bacteria adhere to the implant surface, followed by aggregation and biofilm formation. The biofilm embeds microorganisms in a matrix of polysaccharides, extracellular DNA, and proteins, thus increasing the resistance to both antibiotics and host immune response [59]. Simvastatin inhibited biofilm formation by *S. epidermidis* and *S. aureus in vitro*

at MIC. At 4×MIC, simvastatin significantly destroyed the established biofilms of *S. epidermidis* and *S. aureus in vitro* compared to the control group.

The bioavailability of orally administered simvastatin is low due to first-pass metabolism in the liver, which is the main source of cholesterol synthesis. Our previous studies proved that local application of simvastatin could improve osteoporosis in ovariectomized rats [60]. Local application of single-dose simvastatin improved implant fixation by increasing angiogenesis and bone formation in an ovariectomized rat model [14]. We further utilized electrochemical deposition to generate simvastatin-hydroxyapatite coated Ti6Al4V to combat IAIs. SEM, XRD, and FTIR results confirmed that the Sim-HA coatings were successfully deposited on the surface of the Ti6Al4V implants. The drug release process was similar to that reported in a previous study using an HA coating to integrate drugs [61]. Approximately 50% of simvastatin was released in the first 24 h and the remaining was released slowly from the Sim-HA coatings over 14 days. These results indicated the potential immediate and long-lasting antibacterial effects of Sim-HA coatings, which were proven in subsequent *in vitro* and *in vivo* experiments.

Thus, we investigated the antibacterial effects of Sim-HA coatings *in vitro*. Sim-HA coatings inhibited the bacterial growth and biofilm formation of *S. aureus* on Ti6Al4V *in vitro*. These results are consistent with the antibacterial and anti-biofilm effects of simvastatin *in vitro*. Recently, Esther investigated whether statins could decrease antibiotic resistance and resensitize MRSA to traditional antibiotic treatments by interfering with lipid biosynthesis of membrane microdomains, and thereby disassembling bacterial functional membrane microdomains [13].

The mechanisms underlying the action of simvastatin on bacterial lipid biosynthesis, which contribute to its anti-biofilm effect, require further investigation. Additionally, the Sim-HA coatings inhibited bacterial adhesion. Bacterial adhesion onto the surface of implants is the earliest step of infection; bacteria begin to proliferate after firmly adhering to the surface [62]. The wettability, roughness, and microstructure of the surface affect bacterial adhesion [48,63]. Sim-HA coatings decreased the contact angle of the control and HA groups. One of the reasons for this decrease is that the hydrophilic form of simvastatin [26,64] was used to generate Sim-HA coatings on the implants. In addition, the roughness results were consistent with the change in the contact angles. Extremely hydrophobic or an extremely hydrophilic surface reduced bacterial adhesion on polymeric substrates [65]. Surface roughness could promote hydrophilicity, inhibiting bacterial adhesion by discouraging hydrophobic interactions and creating substrate-bacteria repulsion. The changes in wettability and roughness, as well as the antibacterial effects of simvastatin, may account for the inhibition of bacterial adhesion and subsequent biofilm formation on Sim-HA coatings.

We further evaluated the effects of Sim-HA coatings on the biocompatibility of Ti6Al4V implants. According to our results, Sim-HA-Ti6Al4V improved rat BMSCs adhesion, expansion, proliferation, and osteogenic differentiation on the surface compared with the control groups. An increase in wettability and roughness of the surface can improve the biocompatibility of implants [66]. The ALP activity of BMSCs on the Sim-HA coatings was significantly higher than that in the control and HA groups, reflecting the promotion of osteogenic differentiation at an early stage. Consequently, the improved biocompatibility of Ti6Al4V by Sim-HA coatings played a very good expectation and verification for bone formation and osteointegration *in vivo*. Collectively, the results of the *in vitro* experiments showed that Sim-HA-Ti6Al4V exhibited both antibacterial activity and improved biocompatibility characteristics.

We then established a rat femur IAI model with intramedullary administration of *S.aureus* to evaluate the antibacterial and osteogenic effects of Sim-HA-Ti6Al4V *in vivo* with a number of distinct experiments. The antibacterial effects of the Sim-coatings mainly contributed to the inhibition of biofilm formation on the implant surface, indicating the preventive property of coated implants in the IAI model. The levels of

pro-inflammatory cytokines IL-6 and TNF-α decreased in the Sim-coated groups compared to those in the control and HA groups. The potential anti-inflammatory or immune-adaptive mechanisms of simvastatin in IAI require further investigation.

Gristina. et al. reported that bacterial adhesion and tissue cell integration on the same surface of implanted biomaterial competed in the "race to the surface" [67]. Although calcium phosphate coatings have the disadvantage of low elasticity, causing delamination and destruction of the coatings during implantation or bending deformities of implants [68], simvastatin and hydroxyapatite are beneficial to osteogenesis. Sim-HA coatings could improve the osteointegration of implants *in vivo*, which was verified by results of micro-CT and biomechanical pull-out test. The osteogenic effects of Sim-HA coatings may contribute to the inhibition of bone absorption and improvement of bone formation in the IAI model.

Although there were positive *in vitro* and *in vivo* results, the present study had some limitations. The potential mechanisms by which simvastatin inhibits biofilm formation require further investigation both *in vitro* and *in vivo*. Only the preventive effect of Sim-HA-Ti6Al4V was examined, and the effect of Sim-based therapy on IAI with established biofilms needs further evaluation. Finally, whether Sim-HA coatings could resist MRSA related IAI requires further investigation.

## 5. Conclusion

In this study, Sim-HA coatings were successfully fabricated using an electrochemical deposition method. Sim-HA coatings inhibited biofilm formation and improved biocompatibility and bone formation of titanium alloys to prevent orthopedic IAI. These results may provide a novel strategy for constructing bioactive materials with both antibacterial and osteogenic properties for clinical applications.

## Funding

## CRediT authorship contribution statement

**Tiantong Sun:** Conceptualization, Methodology, Investigation, Data curation, Formal analysis, Validation, Visualization, Writing – original draft, Writing – review & editing, Software. **Jie Huang:** Investigation, Visualization, Validation, Methodology. **Wang Zhang:** Visualization, Data curation, Methodology. **Xuanqi Zheng:** Methodology, Formal analysis. **Hong Wang:** Formal analysis, Resources, Writing – review & editing. **Jing Liu:** Methodology, Formal analysis, Resources. **Huijie Leng:** Resources, Writing – review & editing. **Wanqiong Yuan:** Visualization, Writing – review & editing. **Chunli Song:** Conceptualization, Writing – review & editing, Supervision, Project administration, Funding acquisition.

## Declaration of competing interest

None.

## Acknowledgements

## Appendix A. Supplementary data

Supplementary data to this article can be found online at https://doi.org/10.1016/j.bioactmat.2022.07.028.

## References

[1] W. Zimmerli, Clinical presentation and treatment of orthopaedic implant-associated infection, J. Intern. Med. 276 (2) (2014) 111–119.

[2] B.H. Kapadia, R.A. Berg, J.A. Daley, J. Fritz, A. Bhave, M.A. Mont, Periprosthetic joint infection, Lancet 387 (10016) (2016) 386–394.

[3] A.G. Ashbaugh, X. Jiang, J. Zheng, A.S. Tsai, W.S. Kim, J.M. Thompson, et al., Polymeric nanofiber coating with tunable combinatorial antibiotic delivery prevents biofilm-associated infection in vivo, Proc. Natl. Acad. Sci. U. S. A. 113 (45) (2016) E6919–e6928.

[4] M. Vallet-Regi, D. Lozano, B. Gonzalez, I. Izquierdo-Barba, Biomaterials against bone infection, Adv. Healthc. Mater. 9 (13) (2020), e2000310.

[5] W. Zimmerli, P. Sendi, Orthopaedic biofilm infections, Apmis 125 (4) (2017) 353–364.

[6] L. Hall-Stoodley, J.W. Costerton, P. Stoodley, Bacterial biofilms: from the natural environment to infectious diseases, Nat. Rev. Microbiol. 2 (2) (2004) 95–108.

[7] J.E. Shea, S.C. Miller, Skeletal function and structure: implications for tissue-targeted therapeutics, Adv. Drug Deliv. Rev. 57 (7) (2005) 945–957.

[8] M.A. Fernandez-Yague, S.A. Abbah, L. McNamara, D.I. Zeugolis, A. Pandit, M. J. Biggs, Biomimetic approaches in bone tissue engineering: integrating biological and physicomechanical strategies, Adv. Drug Deliv. Rev. (2015) 84.

[9] W. Zhang, C. Sun, J. Zhu, W. Zhang, H. Leng, C. Song, 3D printed porous titanium cages filled with simvastatin hydrogel promotes bone ingrowth and spinal fusion in rhesus macaques, Biomater. Sci. 8 (15) (2020) 4147–4156.

[10] H. Liu, W. Li, C. Liu, J. Tan, H. Wang, B. Hai, et al., Incorporating simvastatin/poloxamer 407 hydrogel into 3D-printed porous TiAlV scaffolds for the promotion of angiogenesis, osseointegration and bone ingrowth, Biofabrication 8 (4) (2016), 045012.

[11] Z. Yu, J. Guo, Y. Liu, M. Wang, Z. Liu, Y. Gao, et al., Nano delivery of simvastatin targets liver sinusoidal endothelial cells to remodel tumor microenvironment for hepatocellular carcinoma, J. Nanobiotechnol. 20 (1) (2022) 9.

[12] L. Xu, X. Sun, G. Zhu, J. Mao, B. Baban, X. Qin, Local delivery of simvastatin maintains tooth anchorage during mechanical tooth moving via anti-inflammation property and AMPK/MAPK/NF-kB inhibition, J. Cell Mol. Med. 25 (1) (2021) 333–344.

[13] E. Garcia-Fernandez, G. Koch, R.M. Wagner, A. Fekete, S.T. Stengel, J. Schneider, et al., Membrane microdomain disassembly inhibits MRSA antibiotic resistance, Cell 171 (6) (2017) 1354–1367 e20.

[14] J. Tan, N. Yang, X. Fu, Y. Cui, Q. Guo, T. Ma, et al., Single-dose local simvastatin injection improves implant fixation via increased angiogenesis and bone formation in an ovariectomized rat model, Med. Sci. Mon. Int. Med. J. Exp. Clin. Res. 21 (2015) 1428–1439.

[15] C. Yueyi, H. Xiaoguang, W. Jingying, S. Quansheng, T. Jie, F. Xin, et al., Calvarial defect healing by recruitment of autogenous osteogenic stem cells using locally applied simvastatin, Biomaterials 34 (37) (2013) 9373–9380.

[16] M. Schachter, Chemical, pharmacokinetic and pharmacodynamic properties of statins: an update, Fund. Clin. Pharmacol. 19 (1) (2005) 117–125.

[17] J. Zhu, C. Zhang, J. Jia, H. Wang, H. Leng, Y. Xu, et al., Osteogenic effects in a rat osteoporosis model and femur defect model by simvastatin microcrystals, Ann. N. Y. Acad. Sci. 1487 (1) (2021) 31–42.

[18] W. Zhang, C. Sun, J. Zhu, W. Zhang, H. Leng, C. Song, 3D printed porous titanium cages filled with simvastatin hydrogel promotes bone ingrowth and spinal fusion in rhesus macaques, Biomater. Sci. 8 (15) (2020) 4147–4156.

[19] X. Fu, J. Tan, C.G. Sun, H.J. Leng, Y.S. Xu, C.L. Song, Intraosseous Injection of Simvastatin in poloxamer 407 hydrogel improves pedicle-screw Fixation in ovariectomized minipigs, J. Bone Joint Surg. 98 (22) (2016) 1924–1932.

[20] P.M. da Silva Filho, A.L. Andrade, J.B.A.C. Lopes, A.d.A. Pinheiro, M.A. de Vasconcelos, S.G.d.C. Fonseca, et al., The biofilm inhibition activity of a NO donor nanosilica with enhanced antibiotics action, Int. J. Pharm. 610 (2021), 121220.

[21] S. Thangamani, H. Mohammad, M.F. Abushahba, M.I. Hamed, T.J. Sobreira, V. E. Hedrick, et al., Exploring simvastatin, an antihyperlipidemic drug, as a potential topical antibacterial agent, Sci. Rep. 5 (2015) 16407.

[22] H.H.T. Ko, R.R. Lareu, B.R. Dix, J.D. Hughes, In vitro antibacterial effects of statins against bacterial pathogens causing skin infections, Eur. J. Clin. Microbiol. Infect. Dis. 37 (6) (2018) 1125–1135.

[23] S. Thangamani, W. Younis, M.N. Seleem, Repurposing ebselen for treatment of multidrug-resistant staphylococcal infections, Sci. Rep. 5 (2015) 11596.

[24] Z. Shifang, S. Jue, H. Fuming, L. Liu, Y. Guoli, Design and in vitro evaluation of simvastatin-hydroxyapatite coatings by an electrochemical process on titanium surfaces, J. Biomed. Nanotechnol. 10 (7) (2014) 1313–1319.

[25] W. Fang, S. Zhao, F. He, L. Liu, G. Yang, Influence of simvastatin-loaded implants on osseointegration in an ovariectomized animal model, Biomed. Res. Int. (2015), 831504.

[26] A. Laskus-Zakrzewska, P. Kazimierczak, J. Kolmas, Porous composite granules with potential function of bone substitute and simvastatin releasing system: a preliminary study, Materials 14 (17) (2021).

[27] R. Hu, C. Lin, H. Shi, H. Wang, Electrochemical deposition mechanism of calcium phosphate coating in dilute Ca–P electrolyte system, Mater. Chem. Phys. 115 (2–3) (2009) 718–723.

[28] W. Zhou, T. Bai, L. Wang, Y. Cheng, D. Xia, S. Yu, et al., Biomimetic AgNPs@ antimicrobial peptide/silk fibroin coating for infection-trigger antibacterial capability and enhanced osseointegration, Bioact. Mater. 20 (2022) 64–80.

[29] S. Chen, P. Wan, B. Zhang, K. Yang, Y. Li, Facile fabrication of the zoledronate-incorporated coating on magnesium alloy for orthopaedic implants, J. Orthop. Translat. 22 (2020) 2–6.

[30] S.G. Rotman, K. Thompson, D.W. Grijpma, R.G. Richards, T.F. Moriarty, D. Eglin, et al., Development of bone seeker-functionalised microspheres as a targeted local antibiotic delivery system for bone infections, J. Orthop. Translat. 21 (2020) 136–145.

[31] H. Qin, H. Cao, Y. Zhao, C. Zhu, T. Cheng, Q. Wang, et al., In vitro and in vivo anti-biofilm effects of silver nanoparticles immobilized on titanium, Biomaterials 35 (33) (2014) 9114–9125.

[32] W. Zhou, X. Peng, Y. Ma, Y. Hu, Y. Wu, F. Lan, et al., Two-staged time-dependent materials for the prevention of implant-related infections, Acta Biomater. 101 (2020) 128–140.

[33] Y. Yang, H.-Y. Ao, S.-B. Yang, Y.-G. Wang, W.-T. Lin, Z.-F. Yu, et al., In vivo evaluation of the anti-infection potential of gentamicin-loaded nanotubes on titania implants, Int. J. Nanomed. 11 (2016) 2223–2234.

[34] M. Wang, H. Li, Y. Yang, K. Yuan, F. Zhou, H. Liu, et al., A 3D-bioprinted scaffold with doxycycline-controlled BMP2-expressing cells for inducing bone regeneration and inhibiting bacterial infection, Bioact. Mater. 6 (5) (2021) 1318–1329.

[35] Y. Zhuang, L. Ren, S. Zhang, X. Wei, K. Yang, K. Dai, Antibacterial effect of a copper-containing titanium alloy against implant-associated infection induced by methicillin-resistant Staphylococcus aureus, Acta Biomater. 119 (2021) 472–484.

[36] B.e. Nie, H. Ao, T. Long, J. Zhou, T. Tang, B. Yue, Immobilizing bacitracin on titanium for prophylaxis of infections and for improving osteoinductivity: an in vivo study, Colloids Surf. B Biointerfaces 150 (2017) 183–191.

[37] L. Zhu, J. Yang, J. Gong, C. Zhang, B. Ganss, H. Wang, Early bone formation in mini-lateral window sinus floor elevation with simultaneous implant placement: an in vivo experimental study, Clin. Oral Implants Res. 32 (4) (2021) 448–459.

[38] C. Zhang, J. Zhu, J. Jia, Z. Guan, T. Sun, W. Zhang, et al., Effect of single versus multiple fractures on systemic bone loss in mice, J. Bone Miner. Res. 36 (3) (2021) 567–578.

[39] H. Wang, Q. Xu, H. Hu, C. Shi, Z. Lin, H. Jiang, et al., The fabrication and function of strontium-modified hierarchical micro/nano titanium implant, Int. J. Nanomed. 15 (2020) 8983–8998.

[40] A.V. Popkov, E.N. Gorbach, N.A. Kononovich, D.A. Popkov, S.I. Tverdokhlebov, E. V. Shesterikov, Bioactivity and osteointegration of hydroxyapatite-coated stainless steel and titanium wires used for intramedullary osteosynthesis, Strat. Trauma Limb Reconstr. 12 (2) (2017) 107–113.

[41] H. Liu, Y. Tang, S. Zhang, H. Liu, Z. Wang, Y. Li, et al., Anti-infection mechanism of a novel dental implant made of titanium-copper (TiCu) alloy and its mechanism associated with oral microbiology, Bioact. Mater. 8 (2022) 381–395.

[42] X. Zhang, G. Zhang, M. Chai, X. Yao, W. Chen, P.K. Chu, Synergistic antibacterial activity of physical-chemical multi-mechanism by TiO(2) nanorod arrays for safe biofilm eradication on implant, Bioact. Mater. 6 (1) (2021) 12–25.

[43] D. Keskin, G. Zu, A.M. Forson, L. Tromp, J. Sjollema, P. van Rijn, Nanogels: a novel approach in antimicrobial delivery systems and antimicrobial coatings, Bioact. Mater. 6 (10) (2021) 3634–3657.

[44] X. Ge, C. Ren, Y. Ding, G. Chen, X. Lu, K. Wang, et al., Micro/nano-structured TiO (2) surface with dual-functional antibacterial effects for biomedical applications, Bioact. Mater. 4 (2019) 346–357.

[45] X. Qu, H. Yang, B. Jia, M. Wang, B. Yue, Y. Zheng, et al., Zinc alloy-based bone internal fixation screw with antibacterial and anti-osteolytic properties, Bioact. Mater. 6 (12) (2021) 4607–4624.

[46] C. Gao, Y. Wang, F. Han, Z. Yuan, Q. Li, C. Shi, et al., Antibacterial activity and osseointegration of silver-coated poly(ether ether ketone) prepared using the polydopamine-assisted deposition technique, J. Mater. Chem. B 5 (47) (2017) 9326–9336.

[47] H. Zhou, S. Yang, D. Wei, C. Liang, Q. Yang, H. Yang, et al., Development of hydrofluoric acid-cleaned silicon nitride implants for periprosthetic infection eradication and bone regeneration enhancement, Mater. Sci. Eng. C Mater. Biol. Appl. 127 (2021), 112241.

[48] M. Wang, T. Tang, Surface treatment strategies to combat implant-related infection from the beginning, J. Orthop. Translat. 17 (2019) 42–54.

[49] P.S. Zieliński, P.K.R. Gudeti, T. Rikmanspoel, M.K. Włodarczyk-Biegun, 3D printing of bio-instructive materials: toward directing the cell, Bioact. Mater. 19 (2023) 292–327.

[50] Q. Wang, W. Wang, Y. Li, W. Li, L. Tan, K. Yang, Biofunctional magnesium coating of implant materials by physical vapour deposition, Biomater. Transl. 2 (3) (2021) 248–256.

[51] T. Zhang, Q. Wei, H. Zhou, W. Zhou, D. Fan, X. Lin, et al., Sustainable release of vancomycin from micro-arc oxidised 3D-printed porous Ti6Al4V for treating methicillin-resistant Staphylococcus aureus bone infection and enhancing osteogenesis in a rabbit tibia osteomyelitis model, Biomater. Sci. 8 (11) (2020) 3106–3115.

[52] A. Endo, A gift from nature: the birth of the statins, Nat. Med. 14 (10) (2008) 1050–1052.

[53] T.J. LaRocca, P. Pathak, S. Chiantia, A. Toledo, J.R. Silvius, J.L. Benach, et al., Proving lipid rafts exist: membrane domains in the prokaryote Borrelia burgdorferi have the same properties as eukaryotic lipid rafts, PLoS Pathog. 9 (5) (2013), e1003353.

[54] D. Lopez, R. Kolter, Functional microdomains in bacterial membranes, Genes Dev. 24 (17) (2010) 1893–1902.

[55] T.S. Graziano, M.C. Cuzzullin, G.C. Franco, H.O. Schwartz-Filho, E.D. de Andrade, F.C. Groppo, et al., Statins and antimicrobial effects: simvastatin as a potential drug against Staphylococcus aureus biofilm, PLoS One 10 (5) (2015), e0128098.

[56] E. Hennessy, C. Adams, F.J. Reen, F. O'Gara, Is there potential for repurposing statins as novel antimicrobials? Antimicrob. Agents Chemother. 60 (9) (2016) 5111–5121.

[57] L. Dang, J. Zhu, C. Song, The effect of topical administration of simvastatin on entochondrostosis and intramembranous ossification: an animal experiment, J. Orthop. Translat. 28 (2021) 1–9.

[58] P.C. Chang, W.C. Tai, H.T. Luo, C.H. Lai, H.H. Lin, Z.J. Lin, et al., Core-Shell poly-(D,l-Lactide-co-Glycolide)-chitosan Nanospheres with simvastatin-doxycycline for periodontal and osseous repair, Int. J. Biol. Macromol. 158 (2020) 627–635.

[59] M. Idrees, S. Sawant, N. Karodia, A. Rahman, Staphylococcus aureus biofilm: morphology, genetics, pathogenesis and treatment strategies, Int. J. Environ. Res. Publ. Health 18 (14) (2021).

[60] N. Yang, Y. Cui, J. Tan, X. Fu, X. Han, H. Leng, et al., Local injection of a single dose of simvastatin augments osteoporotic bone mass in ovariectomized rats, J. Bone Miner. Metabol. 32 (3) (2014) 252–260.

[61] K. Rajesh, S. Ghosh, A. Islam, M.K. Rangaswamy, S. Haldar, P. Roy, et al., Multilayered porous hydroxyapatite coating on Ti6Al4V implant with enhanced drug delivery and antimicrobial properties, J. Drug Deliv. Sci. Technol. 70 (2022), 103155.

[62] Y.H. An, R.J. Friedman, Concise review of mechanisms of bacterial adhesion to biomaterial surfaces, J. Biomed. Mater. Res. 43 (3) (1998) 338–348.

[63] X.-Q. Dou, D. Zhang, C. Feng, L. Jiang, Bioinspired hierarchical surface structures with tunable wettability for regulating bacteria adhesion, ACS Nano 9 (11) (2015) 10664–10672.

[64] C. Canal, K. Khurana, S. Gallinetti, S. Bhatt, J. Pulpytel, F. Arefi-Khonsari, et al., Design of calcium phosphate scaffolds with controlled simvastatin release by plasma polymerisation, Polymer 92 (2016) 170–178.

[65] Y. Yuan, M.P. Hays, P.R. Hardwidge, J. Kim, Surface characteristics influencing bacterial adhesion to polymeric substrates, RSC Adv. 7 (23) (2017) 14254–14261.

[66] M. Nakazawa, M. Yamada, M. Wakamura, H. Egusa, K. Sakurai, Activation of osteoblastic function on titanium surface with titanium-doped hydroxyapatite nanoparticle coating: an in vitro study, Int. J. Oral Maxillofac. Implants 32 (4) (2017) 779–791.

[67] A.G. Gristina, Biomaterial-centered infection: microbial adhesion versus tissue integration, Science (New York, N.Y.) 237 (4822) (1987) 1588–1595.

[68] E.N. Bolbasov, A.V. Popkov, D.A. Popkov, E.N. Gorbach, I.A. Khlusov, A. S. Golovkin, et al., Osteoinductive composite coatings for flexible intramedullary nails, Mater. Sci. Eng. C Mater. Biol. Appl. 75 (2017) 207–220.